2017 Department of Defense – Allied Nations Technical Corrosion Conference

Paper No. 2017-0000

MODELING GALVANIC CORROSION BEHAVIOR OF CARBON FIBER COMPOSITE/AL 7050 JOINTS UNDER EXTENDED EXPOSURES

Siva Palani, Corrdesa LLC

Alan Rose, Corrdesa LLC

Keith Legg, Corrdesa LLC

Keywords: modeling, galvanic corrosion, polarization curve, carbon fiber composite, Al 7050

INTRODUCTION

The demand for lightweight design and better fuel-efficiency in the aerospace industry has reflected a significant increase in usage of more lightweight materials such as CFC (Carbon Fiber Composite), titanium and aluminum alloys. Combinations of these dissimilar materials are often dictated by structural requirements that need to be fulfilled in the design. In an aircraft, these disparate materials are usually mechanically joined using fasteners or structural adhesives. However, when CFC and aluminum are connected, galvanic corrosion may be induced in the presence of moisture, introducing an additional degradation mechanism. As a consequence, it is important to investigate the impact of material degradation on overall system performance. A major long term concern is the degradation due to localized corrosion and stress corrosion cracking, especially on high strength 7000 series aluminum alloys. Cracks on aluminum commonly initiate from galvanically-driven corrosion pits around fastener holes, and a U.S. Air Force study [1] concluded that 80% of structural failures originated from corrosion pits. Consequently, there is a strong drive to improve protection from galvanic corrosion and to incorporate these improvements in new designs.

ASTM B117 salt spray test is one of the most widely adopted accelerated corrosion tests for providing an estimate of corrosion resistance, protection and evolution of materials and protective coatings. This method is also often being used to evaluate multi-material assemblies with regards to galvanic corrosion performance. One other established method for the analysis of galvanic corrosion behavior is finite element modeling. Corrosion models have become increasingly relevant for simulation, lifetime prediction, and optimization of corrosion prevention measures. Previous work has shown good agreement between modeling and experiments, which shows that numerical simulation is an appropriate method for the evaluation of real galvanic systems [2-8].

The work reported here focuses on modeling galvanic corrosion behavior between CFC and Al 7050-T7451 couples joined using titanium fasteners. Assemblies were analyzed using the finite-element method, and the simulation results compared against the experimental findings after ASTM B117 constant salt spray exposure testing. Particular attention has been given to electrolyte film thickness and its impact on polarization behavior of the materials and their resulting galvanic activity.

EXPERIMENTAL

Materials

AA7050-T7451 (typically Zn 6.06%, Mg 2.20%, Cu 2.12%, Zr 0.11%, Fe 0.08%, Si 0.04%, balance Al) were cut into 15 cm x 10 cm x 0.6 cm rectangles, some bare and some sulphuric acid anodized (SAA) according to MIL-8625 Type 1. 7.5 cm x 5 cm CFC panels were made from prepreg Type 5 mm plate material. Prepregs are rolls of uncured composite materials in which the fibers have been pre-impregnated (combined) with the resin or polymer i.e. the matrix [9]. Both planar sides of the cut CFC were machined down about 100 microns in order to remove the outer resin layer and expose the surface-parallel carbon fibers to create a defined CFC surface and a worst-case galvanic condition when coupled with aluminum. All samples were degreased with ethanol and air dried. The aluminum and CFC plates were mechanically joined using 4 COTS aerospace HI-LOK™ titanium fasteners comprising a Ti-6Al-4V threaded pin and a Ti-3Al-2.5V collar (nut). To simulate a worst-case scenario these fasteners are installed into the material without sealant in order to force galvanic corrosion. The fastener countersink pin was on the CFC side with the collar on the back portion of the aluminum plate. These types of fasteners are designed to exert a known clamp load, since part of the collar is designed to shear off at a predetermined pre-load torque while fastening. An illustration of the joint and the list of test cases can be visualized in Figure 1 and Table 1 respectively.

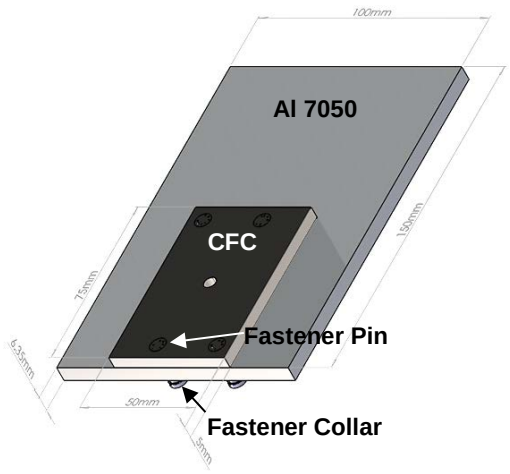

Figure 1. Schematic of the Al 7050/CFC joint with 4 fasteners

ASTM B117 Salt Spray Test

The corrosion behavior of these joints was investigated by static B117 salt spray testing at 35 °C for 4 weeks (28 days), at a reduced salt concentration of 3.5 wt.% NaCl rather than 5 wt.% in order to represent seawater conditions. The samples were suspended in the chamber an angle of 22° from the vertical, with CFC at the bottom, facing forward, with from vertical as shown in Figure 1. Condensate collection volume and pH values were measured daily.

Table 1: List of test cases and conditions

	Material A (15x10 cm)	Material B (7.5x5 cm)	Material C (Fastener Pin)	(Fastener Collar)
Test Case	Al 7050-T7451	CFC	Ti-6Al-4V	Ti-3Al-2.5V
1	Bare	sanded	degreased	degreased
2	Anodized (SAA)	sanded	degreased	degreased

Electrolyte Film thickness

The objective of this work was to model galvanic corrosion behavior of the joint system under salt spray chamber (i.e. thin electrolyte) conditions. Galvanic corrosion under thin electrolyte has different characteristics compared to those of a bulk electrolyte. Under thin electrolytes, corrosion is faster as more oxygen is available for the oxygen reduction reaction at the cathode (CFC or Ti). This is an important point, since it is the cathode oxygen-reduction reaction, not the oxidation reaction on the aluminum, that controls galvanic corrosion. Additionally, in reality at a given moment the film thickness is expected to vary depending mainly on the geometry or joint, orientation, material surface chemistry, condition and temperature. Therefore, within the scope of this work in order to come up with the best approximation, a computational fluid dynamics (CFD) analysis was carried in order to simulate the electrolyte film formation on the joint under constant high humidity conditions. Based on this analysis, a universal film thickness of 60 µm was found to be a best approximation in order to acquire the required polarization data for modelling. The details on this CFD analysis will be discussed in a later section of this work.

Electrochemical Polarization Measurement

When modeling a galvanic system, it is very important to know and understand the actual test or service condition with which it will be compared. In this case, the polarization data (especially for the CFC) must be representative of thin film conditions. Since it is difficult to measure polarization data with thin electrolyte films, a Rotating Disk Electrode (RDE) technique was used to generate the experimental potentiodynamic polarization curves for the CFC. Through this well-defined method, stable mass transport is achieved via convection–diffusion. As an approximation for the cathodic reaction on the CFC, the film thickness is assumed to be represented by the oxygen diffusion layer of a controlled homogenous hydrodynamic interface. So, in an RDE the diffusion layer thickness,

δ, could be calculated based on the rotation speed ω. The relationship between δ and ω is given by [10]:

$$\delta = 1.61 D^{1/3} \upsilon^{1/6} \omega^{-1/2} \quad (1)$$

with

D : Diffusion coefficient of oxygen at 35˚C, 2.92x10^{-9} [m².s^{-1}]

υ : Kinematic viscosity of water at 35˚C, 7.12x10^{-4} [Pa.s]

D is the diffusion coefficient of oxygen in water calculated from literature data based on the Stokes–Einstein equation [11], and υ is the kinematic viscosity of water calculated from literature data [12]. Aluminum polarization data were all taken under bulk electrolyte conditions, since Al is an anode in this galvanic system and the thickness of the diffusion layer should not influence the anodic behavior. Fasteners polarization data were acquired from the titanium fasteners that were used, i.e. the pin and the collar and were of necessity taken under bulk conditions. The bulk polarization curves of the titanium fasteners where refitted incorporating the recalculated diffusion-limited oxygen reduction current density that corresponds to 60 µm, based on Fick's 1st law [13]. All the curves were taken in 3.5 wt.% NaCl at 35˚C in near-neutral pH starting from open circuit potential. These curves served as input data for the model of the cases as shown in Table 1.

Finite element modeling

The geometry shown in Figure 1 was created in SolidWorks 2016. Then the finite element modeling was carried on Elsyca Corrosion Master software, which uses a thin film approach. With this model, it is assumed that the entire surface area of all components involved in the simulation are covered with a thin film of uniform thickness and constant conductivity. The software automatically calculates the overlap between thin films on different bodies to ensure ion transfer between neighboring bodies with overlapping films.

Governing equations

The mathematical formulation is based on the potential model. Ohm's law describes the current density proportional to the electric field, E:

$$\sigma\vec{E} = -\sigma \cdot \vec{\nabla} U \quad (2)$$

$\vec{E}$: Electric field [V/m]
σ : Conductivity [Ω^{-1}m^{-1}]
U : Potential [V]

with the proportionality factor being the conductivity. Expressing current conservation in local form yields the Laplace-equation which is a partial differential equation of second order law [14].

$$\vec{\nabla} \cdot (-\sigma \cdot \vec{\nabla} U) = 0 \quad (3)$$

The electrolyte is treated as a homogeneous ohmic conductor with no ion diffusion or convection effects. Additionally, the model treats the problem with the assumption that the potential in the electrolyte is almost constant along the thickness of the film (i.e., normal direction to the material face) as the electrolyte film gets very thin. This allows the model to treat it as a two-dimensional problem, reducing the Laplace equation to:

$$\vec{\nabla}_{2D} \cdot (-\sigma \vec{\nabla}_{2D} U) = -f(U) \quad (4)$$

where $\vec{\nabla}_{2D}$ is the 2-D gradient operator solving for x, y-coordinates and $f(U)$ is the imposed polarization curve, which serves as the boundary condition. Eq. (4) is solved using FEM to numerically discretize the geometry and solve to obtain current density and potential at all the nodes on all the materials.

Laser Profilometry

At the end of the 28-day salt spray test, the galvanic joints were rinsed in deionized water and the all the corrosion products removed with a 3M Scotch-Brite© pad. The assembly was allowed to air dry at ambient conditions. The joint was then mounted on a tri-cell adjustable stage for optical surface profiling (OSP) measurements using a BioLogic M470 scanning electrochemical workstation with an OSP laser with a step size of 50 µm in both x and y axes.

RESULTS AND DISCUSSION

Polarization Behavior

Figure 2 displays the potentiodynamic polarization curves for all the materials involved. Clearly the CFC and titanium are electrochemically nobler than Al 7050 bare and anodized. The Al 7050 bare anodic curve shows that its pitting potential is at open circuit potential (OCP). The anodized Al 7050 has a very similar OCP. The CFC, on the other hand, is strongly cathodic both on the top and the cross section, resulting in very high cathodic current densities. The point where the CFC cathodic curve crosses the Al 7050 anodic curve indicates the galvanic coupling current density. In this case, the galvanic coupling current density is an order of magnitude higher than the self-corrosion current density of Al 7050, i.e. the galvanic corrosion rate will be ~10x the self-corrosion rate. The Ti-6Al-4V pin showed rather low kinetics in comparison to the CFC. But the Ti-3Al-2.5V fastener collar

showed considerably higher cathodic reaction kinetics, which would result in a very high galvanic current coupling current density comparable to the CFC. This is a serious issue for structures if the wrong material is used for any part of the fastener that couples to the aluminum.

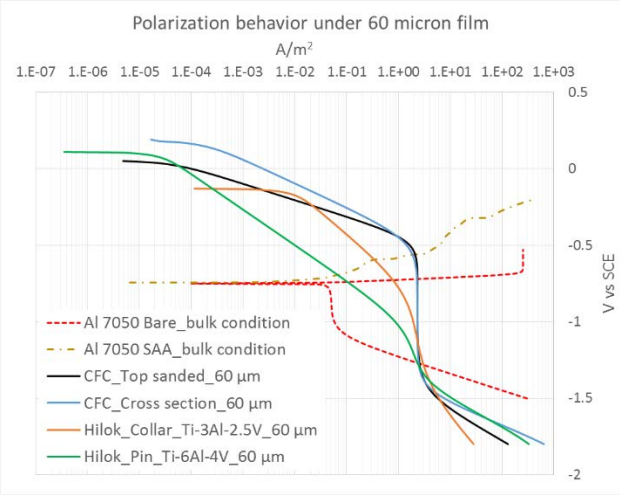

Figure 2. Potentiodynamic polarization curves of materials used in the joint under 60 micron 3.5 wt.% NaCl film, at 35˚C

Salt Spray Testing

Figure 3 shows the galvanic assembly before and after 4 weeks of constant 3.5 wt.% salt spray exposure. Many pits have formed all over the exposed bare aluminum in the Test Case 1 assembly, and the pit density is very high all along the interface area close to the cut edge of CFC plate, where the ends of the fibers are completely exposed. In Test Case 2 with anodized aluminum, pitting still occurred but it was localized along the interface area very close to the cut edge of the CFC plate. The pits that occurred on areas away from the CFC and along the edges of the anodized aluminum could be associated with imperfect anodized layer which became the pit initiation point. There was also corrosion found on aluminum around the area where the fastener collar is in contact at the back of the assembly on both the test cases. This is due to higher cathodic kinetics of the Ti-3Al-2.5V fastener collar.

Pit depth evaluation

Two-dimensional area optical surface scans were carried out on 2 locations, Area A and B on both the assemblies. The red boxes in Figure 3 mark the scan locations and size on each assembly. The anodized aluminum in Test Case 2, which in this case exhibited less corrosion away from the CFC plate, required a smaller scan area. Based on the measured depth profile and scan step interval, the volume loss on aluminum due to anodic dissolution was calculated by subtracting the measured average height of a non-corroded surface on aluminum.

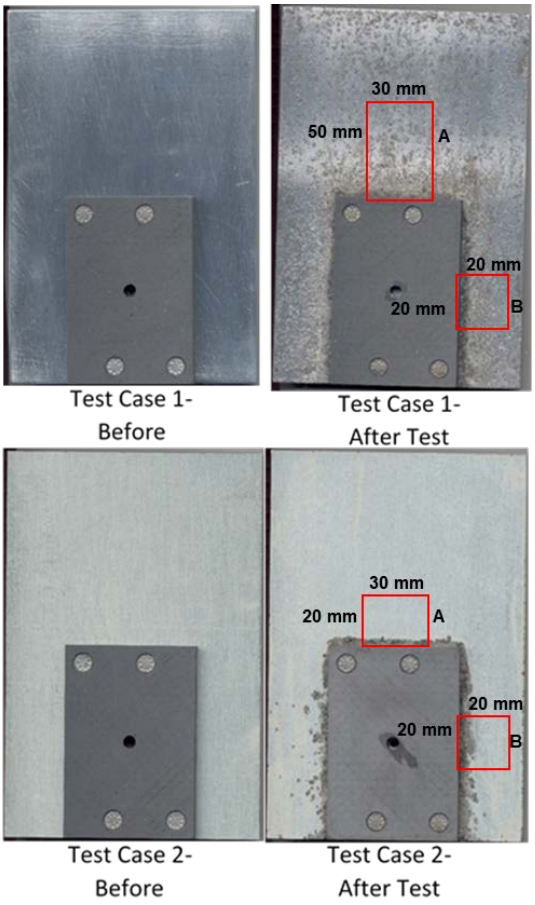

Figure 3. Galvanic test assembly. Top bare Al, bottom anodized, before and after 28 days of B117 exposure.

Figure 4 and Figure 5 show the 2-D and 3-D maps of the pitted bare and anodized aluminum 7050 close to edge of the CFC. From the graph, it is evident that strong galvanic interaction with CFC along the top interface (Area A) has caused severe aluminum dissolution which was rather uniform. The deepest corrosion depth at Area A was measured to be around 400 µm very close to the CFC interface. At the side (Area B), the corrosion looked rather less uniform, with large, deep pits scattered along the side CFC interface, with the deepest corrosion being about 530 µm, as shown in Figure 4. Figure 5 shows equivalent data for the anodized galvanic assembly. Anodizing almost entirely prevents the self-corrosion that we see across the entire surface of the bare aluminum, but a very narrow, deep line of corrosion pits formed on the aluminum at the top surface of the composite, with a broader area of large random pits down the sides, measuring almost 500µm deep.

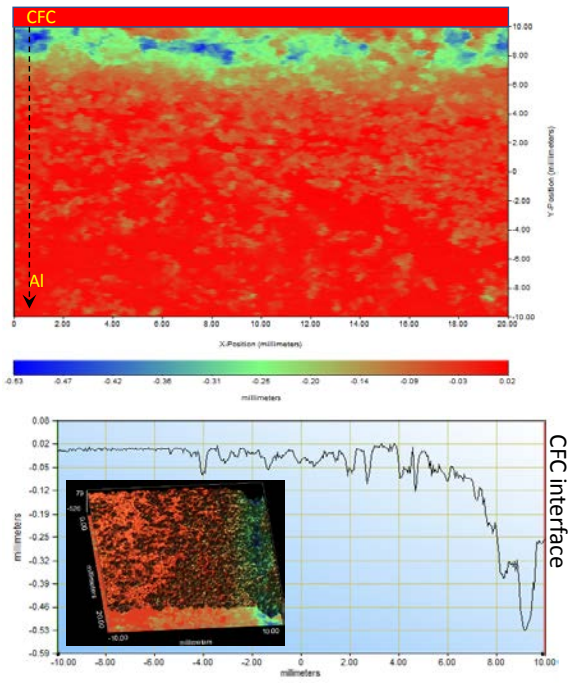

Figure 4. 2D surface profile map of Test Case 1 (bare aluminum), area B.

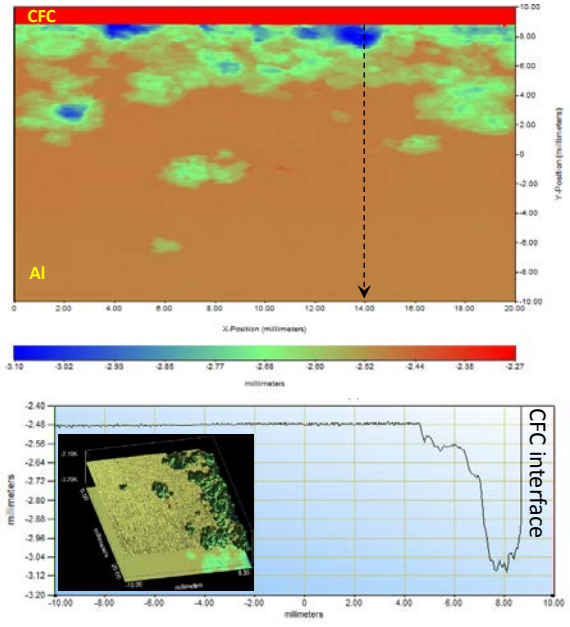

Figure 5. 2D surface profile map of Test Case 2 (anodized aluminum), area B.

Modeling

Computational Fluid Dynamics modeling

Accelerated corrosion tests such as B117, GMW 14872, ISO 21207:2015, for example, are extensively used as tools to help designers make choices on appropriate materials. Since these tests are aimed at *accelerating* corrosion there is much debate as to whether the *correct* mechanisms are actually accelerated. Whatever the corrosion environment, an electrolyte must always be present, and in the case of atmospheric corrosion, the electrolyte film can be very thin indeed. Before we can start to simulate corrosion, we must know the thickness of the electrolyte, since this is a key parameter which controls the corrosion rate. A very thin electrolyte allows easier access of oxygen to the substrate beneath, and creates a larger IR (resistive) drop, which impacts the distribution of potential and current density.

The thickness of the film greatly depends on relative humidity, the shape of the surface, presence of contaminants and many other factors such as temperature, sunlight exposure etc. So, what thickness should be used in galvanic corrosion simulations? Much can be learned from Nusselt's treatment of thin film condensation on a vertical wall (Figure 6).

By balancing the assumed conductive heat transfer from the film surface to the wall with the enthalpy of evaporation for the mass flow down the wall, Nusselt was able to derive an expression for the thickness profile of the condensate film down the vertical wall. This was extended to the case of an inclined plane;

$$\delta(z) = \left[\frac{4\mu k(T_s - T_w)}{\rho(\rho_L - \rho_G) g \, sin\alpha \, h_{GL}} \mathrm{Z}\right]^{1/4}$$

Where

δ : Local film thickness [m]
T : Temperature (saturated; wall) [˚C]
ρ : Mass density (liquid; gas) [kg.m-3]
μ : Viscosity (liquid) [kg.m-1.s-1]
g : Gravity acceleration [m.s-2]
k : Thermal conductivity (liquid) [W.m-1]
z : z-coordinate point from top of the plate [m]
h : Latent heat [kJ.kg-1]
α : Angle relative to horizontal

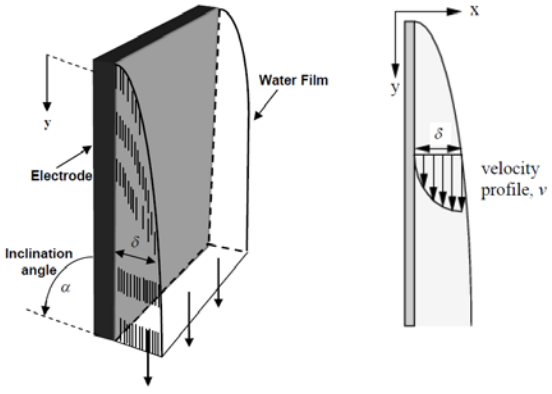

Figure 6. Nusselt treatment of fluid flow down a plate.

For calculation of fluid film thickness distribution over more complex shapes we use the CFD software CD-

Adapco CCM+ (STAR-CCM+ v12.02.011-R8 for Windows 64). CCM+ has an implementation of a fluid film model which, using a transient solver, accounts for transport of conserved quantities within the film and its interaction with surroundings considering conservation of mass, momentum, energy and species (Figure 7). A key assumption is that the film is thin enough for laminar boundary layer approximation to apply, resulting in a parabolic velocity profile across the film. This enables the simulation of evaporation and condensation, leading to film thickness predictions. However, in B117 test the assembly will experience dropwise film condensation on pristine surface at least during the initial stage of exposure and more filmwise condensation as the surface gets corroded.

As a verification exercise, a CCM+ model was made for a simple, inclined flat plate which showed a close match with the use of Nusselt's equation, Figure 7.

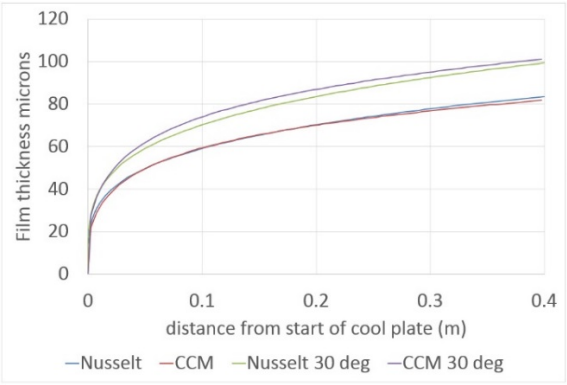

Figure 7. Comparison between CAE and Nusselt.

Having established the thin film simulation methodology in CCM+, we then created the Al/CFC geometry with the same dimensions as the test specimen, but at this juncture, without the fasteners or the drilled hole. The predicted film thickness distribution for the specimen oriented 22° from the vertical, as in the B117 test, is shown in Figure 8.

The full model and simulation details are out of the scope of this particular paper. However, the resulting flow is very interesting and provides insight into what film thicknesses we should assume reasonable for galvanic corrosion simulations. From Figure 8 we see that the film flow is essentially dynamic and, on close observation quite complex. On the back side of the specimen the film can be seen to develop in thickness from zero at the top edge of the aluminum to a little over 60µm at the bottom edge of the specimen. However, on the front side of the specimen, the film thickness develops to about 50µm and is interrupted by the 'step' geometry created by the presence of the CFC, forcing the film to rapidly thicken beyond 1mm, spill over the CFC and then start to develop again. Furthermore, the film is also seen to thicken to about 100 µm very close to the Al/CFC interface down the vertical edges of the CFC.

Using this variable fluid film thickness distribution and a uniform electrical conductivity of 5 S/m, appropriate for a 3.5% NaCl solution, CCM+ was used to calculate the electric potential distribution. The polarization curves for the Al alloy and the CFC were used to set the boundary conditions on the respective surfaces, resulting in a prediction of current density distribution, which was then compared with a simulation assuming a uniform film thickness.

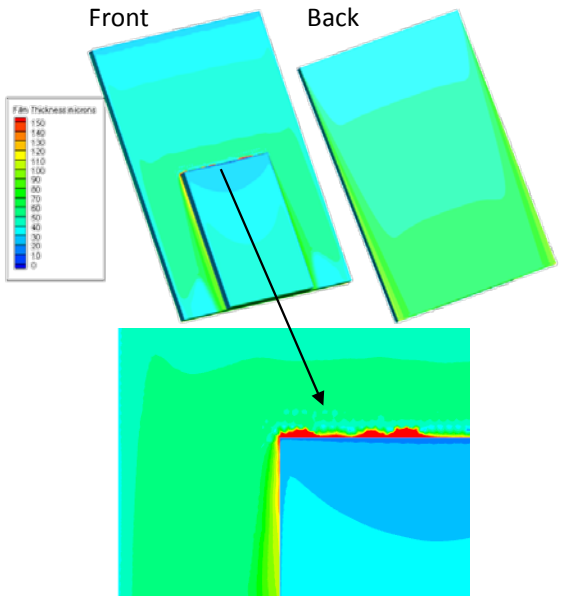

Figure 8. Fluid flow down galvanic assembly.

Galvanic corrosion modeling

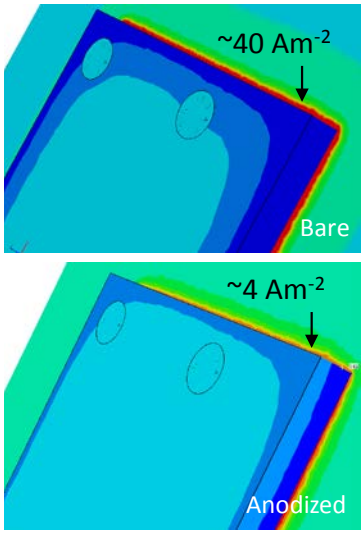

Figure 9. Galvanic current density model of bare and anodized Al corrosion around CFC.

Figure 9 shows the current density on the Al surface around the CFC. Note that the current density is strongly focused at the interface, with the peak current density an order of magnitude higher on the bare Al than the anodized.

Figure 10 shows the galvanic corrosion around the Ti325 collar, which, as Figure 2 shows, has a polarization current more than 10x higher than the more common Ti64. The right of the figure shows the model results and the left shows the deep corrosion around this fastener.

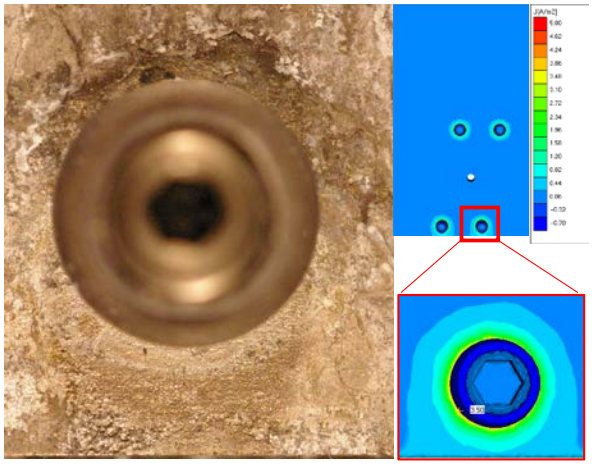

Figure 10. Al corrosion around Ti3Al2.5V collar at back of the assembly after 28 days.

The galvanic corrosion models of Figure 9 and Figure 10 are based on modeling that is restricted to a constant electrolyte thickness and constant polarization curves. However, as we clearly see in Figure 8, the thickness of electrolyte films varies widely around complex assemblies. This has the effect of changing the polarization curve and the IR drop.

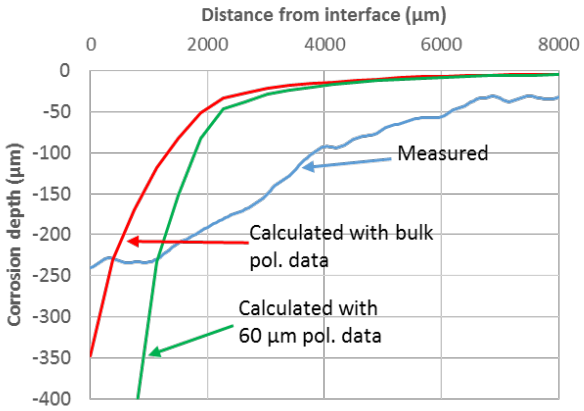

Figure 11. Comparison of measured and calculated corrosion depth vs distance from interface, assuming 60 µm electrolyte film (gray) and thick electrolyte film (red).

In Figure 11 we see that using a model that assumes a constant electrolyte thickness of 60 µm, results in a grossly overestimated corrosion rate and localized at the interface. We have already seen that for complex component shapes the film thickness can vary considerably (Figure 8). Since the electrolyte film on the CFC near the interface is very thick, then it's more appropriate to use the bulk polarization curve at this location, which results in far more accurate prediction of the corrosion rate.

CONCLUSION

Computational modeling is a powerful approach to assessing the long-term corrosion risk in complex assemblies. When assessing galvanic corrosion, it is critical to base the analysis on the galvanic current, not the galvanic potential difference (as MIL-STD-889 currently does).

In the aerospace industry, the most common design practice is to anodize aluminum airframes for optimum corrosion resistance. As Figure 2 and Figure 3 show, anodizing is an effective barrier against self-corrosion of aluminum, but provides little protection against galvanic corrosion, In fact, we see from Figure 5 that anodizing leads to large, deep pits in galvanic regions as galvanic current is concentrated into a few weak points in the anodize layer, instead of being spread across a larger surface area. These pits must be removed on overhaul, leading to excessive loss of structural material.

Although MIL-STD-889 says that it is better to use stainless steel than titanium fasteners with aluminum, galvanic analysis clearly shows the opposite. However, as Figure 2 shows, all titanium alloys are not alike. Using the wrong alloy for any part of the fastener that contacts the aluminum can have serious galvanic corrosion consequences. Choice of each material in a fastener system is therefore critical.

Although simple shapes can be accurately analyzed using assumptions of constant electrolyte thickness, complex shapes require taking into account the thickness of the electrolyte layer around the assembly. Variable electrolyte thickness will also be an important consideration in modeling time-varying corrosion situations such as diurnal variations in humidity and temperature, as well as aiding better understanding and interpretation of accelerated test chamber results.

ACKNOWLEDGEMENTS

This work was sponsored by U.S. Air Force, Walter Juzukonis and ONR, William Nickerson. The views and conclusions contained herein are those of the authors and should not be interpreted as necessarily

representing the official policies or endorsements either expressed or implied, of the US Air Force, ONR or the U.S. Government. We would also like to acknowledge the input from Doug Hansen of UDRI.

REFERENCES

1. G. Shoales, et al., Proc. of the 25th Symposium of the International Committee on Aeronautical Fatigue 2009.
2. S. Palani, T. Hack, J. Deconinck, H. Lohner, Corros. Sci. 78 (2014) 89-100.
3. M. Mandel, L. Krüger, Corros. Sci. 73 (2013) 172-180.
4. K.B. Deshpande, Corros. Sci. 52 (2010) 3514–3522.
5. N. Murer, R. Oltra, B. Vuillemin, O. Néel, Corros. Sci. 52 (2010) 130-139.
6. A. Atrens, J.X. Jia, G. Song, Adv. Eng. Mater. 9 (2007) 65–74.
7. R.G. Kelly, F. Cui, J. Presuel-Moreno, Corros. Sci. 47 (2005) 2987–3005.
8. P. Doig, P.E.J. Flewitt, J. Electrochem. Soc. 126 (1979) 2057-2063.
9. A. Brent, Fundamentals of composites manufacturing: Materials, methods and applications, SME, (2008) 253-255.
10. V.G. Levich, Physicochemical Hydrodynamics, Prentice Hall, Englewood Cliffs, NJ, 1962.
11. Wilke, C. R., P. Chang, Correlation of diffusion coefficients in dilute solutions, A.I.Ch.E. Journal, 1, (1955) 264–270.
12. W.M. Haynes, CRC Handbook of Chemistry and Physics, CRC Press, 2010-2011
13. A. Fick, "Ueber Diffusion". Ann. der Physik (in German) 94 (1855) 59–86.
14. S. Palani, “Modeling of Galvanic Corrosion on Hybrid Structures in Aircraft – application to CFRP-AA2024 unclad material combination”. PhD Thesis, October 2013. Vrije Universiteit Brussel (VUB) Belgium.